Final Deliverables for the ACTIV Code Project
(Project No. 05-07741)

Appendix IV

Summary Results for the
JPDR Activation Analysis Benchmark
Using VITAMIN-B6 and BUGLE96 Data

Summary Results for the JPDR Activation Analysis Benchmark Using VITAMIN-B6 and BUGLE96 Data

Dr. John R. White
Chemical and Nuclear Engineering Department
University of Massachusetts Lowell

August 8, 1997

Introduction

The University of Massachusetts Lowell (UMass-Lowell) was an active participant in an international benchmark exercise organized by the International Atomic Energy Agency (IAEA) to address the adequacy of current cross section data and computational methods for quantifying neutron activation in the excore regions of commercial power reactors.[1] The central focus of the benchmark exercise involved the comparison of calculated results to measured activation data from the Japan Power Demonstration Reactor (JPDR).[2-3] The available experimental data include radial and axial activity profiles at various locations in the excore structure and bioshield regions for several important radioactive isotopes (^{60}Co, ^{54}Mn, ^{55}Fe, etc.). The unique aspect of the UMass-Lowell work was the use of the ACTIV code - a newly-developed space-energy activation analysis capability that takes full advantage of the detailed multigroup information available from a variety of transport theory analyses of the excore regions of power reactors.

The original UMass-Lowell benchmark calculations were completed in 1995 and summary results from that work are given in Ref. 4. The original calculations were based on a 47-group activation analysis library that was derived from a pre-release version of the VITAMIN-B6 library (early 1994 vintage). The transport calculations were done with the BUGLE93 shielding library.[5] In late 1996 an official release of an updated VITAMIN-B6 library was made available through RSICC.[6] In addition the BUGLE shielding library was updated and corrected (there was an error in BUGLE93 in the weighting function used to collapse the neutron cross sections from 199 groups to 47 groups) and released as BUGLE96.[7] On the local level, some minor errors were also found in the original JPDR RZ DORT models used to generate the results in Ref. 4. With all the uncertainty associated with modeling errors, cross section processing errors, and with the impact of an updated base library, it was decided that a complete reanalysis of the JPDR benchmark was certainly needed.

This report briefly overviews the data, methods, models, and codes used to generate the latest JPDR benchmark results and it gives a fairly complete comparison of the computed and measured activities for several isotopes included as part of the JPDR experimental program. Previous works have consistently identified that insufficient geometric and material composition information about the JPDR bioshield lead to poor agreement with measured data in this region.[4, 8-9] Since no new bioshield information is available, the current results emphasize the capability of a DORT-ACTIV sequence to predict long term neutron activation in the excore components up to and including the pressure vessel region. Some data for the surface and

interior of the bioshield are included for future reference, but these data are not considered as part of the DORT-ACTIV verification effort at this time.

Data, Methods, and Codes

The current UMass-Lowell JPDR benchmark computations used the DORT code[10] and the BUGLE96 library[7] for all the 2-D JPDR transport calculations. The BUGLE96 broad-group dataset was collapsed from the ENDF/B-VI VITAMIN-B6 fine-group library[6] with a specific focus on shielding applications. This library is readily available to the user community and it is routinely used for excore radiation transport computations.

The new ACTIV code was used for the activation calculations.[4] This code eliminates much of the uncertainty associated with the use of few-group 'effective' activation cross sections by performing the activation calculations with the same space and energy dependent detail that was used in the transport theory computation for the neutron flux distribution. The same geometry is modeled and the user can select any number of pointwise radial and axial traverses or zone average activations, as desired. Thus, all of the space-energy detail from the original transport computation is preserved and included within the activation calculation – thereby, removing all the additional uncertainty that is introduced in the traditional process (as commonly used with the ORIGEN code,[11] for example).

For full consistency, the activation cross sections used within ACTIV were also derived from VITAMIN-B6. A new ACTXS47.LIB 47-group activation library was generated using several modules of the SCALE 4.3 system,[11] an updated version of ACTXS (a cross section processing code written specifically for generating data for ACTIV),[4] and a newly generated concrete weighting function consistent with that used to develop the BUGLE96 package. Data for eight reaction types (n,γ, n,α, n,p, n,2n, n,d, n,t, n,f, and total neutron absorption) were extracted from the collapsed library and stored in a format suitable for use in ACTIV.

This new activation library is intended for use with a DORT-ACTIV analysis sequence, with the DORT transport calculation based on BUGLE96 cross sections. The BUGLE96 library and the ACTXS47.LIB dataset are both based on VITAMIN-B6 and they have been developed using the same processing methods and assumptions. The two libraries represent a consistent set of data for use in detailed space-energy neutron activation studies. The BUGLE96-DORT calculation determines the appropriate multigroup fluxes and the ACTXS47.LIB-ACTIV computation determines the space and time dependent activities for the desired excore locations.

In addition to the neutron cross sections, natural isotopic abundances, decay data, and appropriate branching fractions are also needed for the activation calculations. These data were obtained from the ENDF/B-VI version of the ORIGEN data libraries that are distributed as part of the SCALE 4.3 package.[11] The necessary data were extracted from the ORIGEN data files and incorporated into the activation library used within ACTIV.

The ACTIV code itself uses the traditional matrix exponential technique for solution of the nuclide transmutation equations. The primary computational algorithms for the matrix exponential method were taken from the DEPTH-CHARGE modules of the VENTURE code system.[12] The ACTIV code simply reads the appropriate nuclide chain information, geometry data, initial isotope densities, and operational power versus time data and, using the precomputed space-energy fluxes from DORT (or some other transport analysis code) and the nuclear data from the activation library, computes the time-dependent isotope inventories for each spatial

point or zone of interest. The data flow and interaction between DORT and ACTIV are illustrated in Fig. 1. The summary edit from ACTIV gives the activity in Bq/g or Ci/g for the desired isotopes, spatial locations, and time points. These data can then be plotted or tabulated for further analyses – which, in the present JPDR benchmark study, involves direct comparison to the measured data from Ref. 2.

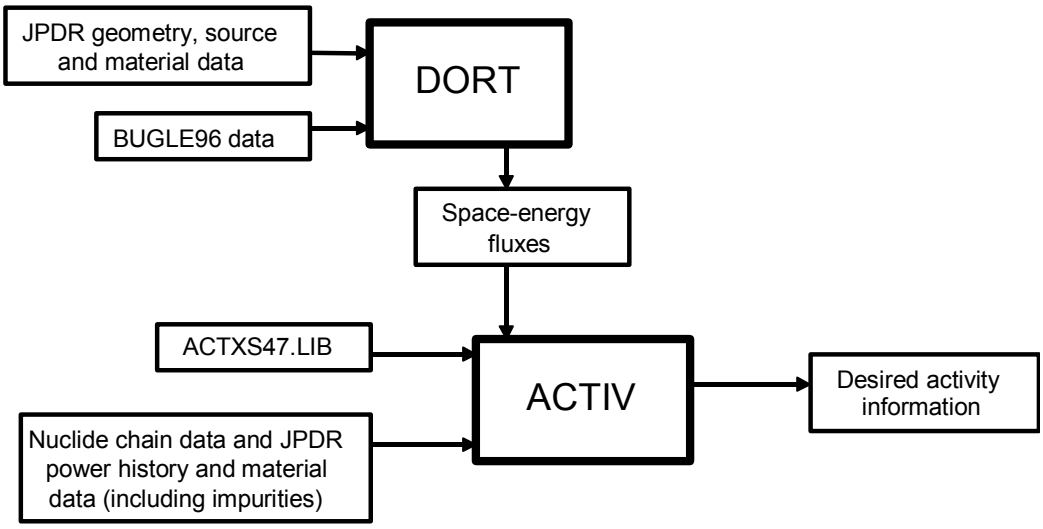

Fig. 1 Data flow and interaction between DORT and ACTIV.

JPDR Modeling within DORT

The Japan Power Demonstration Reactor (JPDR) was a direct-cycle BWR with dimensions that spanned over 12 m axially and 4 m radially. The reactor operated intermittently with varying power level over a period of about 13 years, from 1963 to 1976, with a total reactor thermal output of 21,500 MWD. As outlined in Ref. 4, the 12.2 m axial dimension was broken into three regions and labeled accordingly, with Region 1 at the bottom and Region 3 at the top. A bootstrapping technique, which couples one axial region to another via a saved internal boundary source is envisioned as a mechanism to complete the full benchmark computation. Modeling of the JPDR started at Region 2 which contains the core, and hence, the neutron source which drives the entire model. At present, the Region 2 model is the only computation that has been completed and fully analyzed.

An overall radial dimension of 300 cm was used in the DORT models. Reflected boundary conditions were employed on the left and right model boundaries, and vacuum conditions were imposed on the top and bottom of the Region 2 RZ model.

The final JPDR DORT model has a concrete bioshield containing explicit zones that account for several cooling tubes and structural rebar reinforcements. This model, with an overall 155 x 201 mesh grid, represents an improvement over the initial JPDR configuration documented in Ref. 2 with additional bioshield data from Ref. 3. However, we feel that the bioshield model is still not sufficient for a detailed verification test of the methods. Thus, in the present work, not much emphasis is placed on this region of the JPDR configuration.

The final model here also differs slightly from the one discussed in Ref. 4 in that a finer mesh structure is used in the current model (the Ref. 4 results were based on a computational model with 118 x 123 mesh points) and a single symmetric S_{16} quadrature set is used for the angular discretization (a variable quadrature scheme within DORT was adopted previously to help cut back on the overall computational time). The present model, referred to as Case D, includes the axial region from 90 cm to 509 cm above the bottom of the JPDR reactor vessel. The Case D model geometry was fine tuned slightly (relative to previously reported models) to minimize any numerical uncertainty that may have been introduced by a relatively coarse spatial discretization scheme and the variable quadrature feature.

The final Case D Region 2 JPDR computational model used in this work is illustrated in Fig. 2, where the dark heavy lines represent major material or component boundaries. The material compositions for the various regions highlighted in Fig. 2 for the Case D model were taken directly from Table A.2 in Ref. 2, except for the more explicit modeling in the bioshield region. Table 1 shows the concrete, steel, and water volume fractions used in the Case D bioshield model (these data were derived from Ref. 3). The Zone 1 - 9 designation in the table map to the nine explicit regions identified in Fig. 2 within the bioshield. These are the long narrow zones within the heavy lines and they are numbered from left to right, not counting the concrete liner. The 10^{th} zone in Table 1 is pure concrete and this material occupies all the remaining bioshield regions. The concrete compositions were obtained directly from Ref. 2.

Table 1. Volume fractions for the Case D bioshield model.

		Volume Fractions		
Zone #	Description	Concrete	Steel	Water
1	vertical rebar & cooling pipes w/o water*	0.6928	0.1934	0.0000
2	horizontal rebar	0.8482	0.1518	0.0000
3	vertical cooling pipes with water	0.8466	0.0552	0.0982
4	vertical rebar	0.8841	0.1159	0.0000
5	horizontal rebar	0.8482	0.1518	0.0000
6	vertical rebar	0.9337	0.0663	0.0000
7	horizontal rebar	0.9346	0.0654	0.0000
8	horizontal rebar	0.9346	0.0654	0.0000
9	vertical rebar	0.9333	0.0667	0.0000
10	concrete regions	1.0000	0.0000	0.0000

*Since there is no water within the pipes, the volume fractions sum to less than unity.

Manually insert the mesh structure here

Fig. 2 DORT mesh structure for the JPDR Case D model.

The material composition data for the various regions and the material IDs from the BUGLE96 library were used as part of the mixing table within GIP[10] to create a set of 47-group

macroscopic cross sections for use within the DORT transport calculations. Although scattering expansions up to 5th and 7th order are available within the BUGLE96 library, only P_3 data were used in these benchmark calculations.

The final information necessary to run DORT was the space-energy source distribution within the core region of the JPDR model. Numerical estimates of the spatial source distribution were obtained from Figs. A.2 and A.3 in Ref. 2. A spline fit to the discrete radial and axial profiles produced a continuous distribution and, with this information, the relative source strength associated with the specific mesh spacing utilized in the UMass-Lowell JPDR models was obtained. The actual profiles used are shown in Fig. 3, where the dots indicate the discrete points obtained from the JPDR documentation and the solid lines represent the continuous spline fit. The RZ spatial source distribution is then simply the product of the radial and axial profiles, S(r,z) = S(r)*S(z), evaluated at the midpoints of the mesh volumes used in the DORT model.

The source energy spectrum for the 47-group computations was obtained by integrating the specific Watt fission spectrum given in Ref. 2 over the appropriate 47-group energy grid. The total source was normalized such that 1 MW of thermal power is generated within the core. The actual power level at any specific time is handled within ACTIV via a simple time-dependent normalization of the absolute flux for the 1 MW power case.

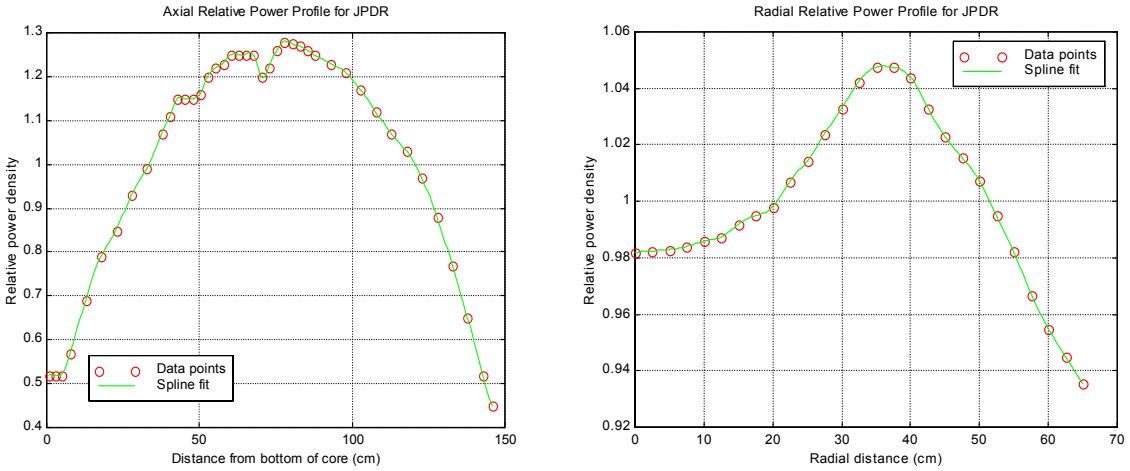

Fig. 3 Relative source profiles used in the Case D JPDR model.

Some DORT Results for the JPDR Region 2 Model

With all the necessary data defined, the DORT calculations were made with a pointwise convergence criterion of 0.001. The full space and energy dependent scalar flux data were saved for subsequent use in ACTIV. In addition, some post-processing of the multigroup flux data – collapsing of the fluxes to three broad groups – was performed for summary presentation of key radial and axial flux profiles. Several multigroup activity cross sections were also collapsed to the three-group level and to a single effective broad group for summary review of the spatial dependence of these 'effective' cross sections versus position within the system. Of particular interest were the few-group flux and cross section profiles in the locations where measured activity data are available. The microscopic reaction rate profiles (reactions per second per

target atom) for several key reactions were also generated from these few-group data. These data can provide considerable insight into the activation analysis problem.

The unique aspect of the ACTIV code is its ability to treat the full space-energy coupling that is inherent in real systems. The transport theory computations produce all the needed neutron distribution information, but all this detail is often ignored or used in an approximate fashion in most analyses. With the availability of a fully compatible multigroup activation library, it becomes a relatively simple process to utilize all the available space-energy detail to eliminate much of the uncertainty that is often associated with most zero-dimensional activation analysis studies (with codes like ORIGEN, for example). As an illustration of some of the information that is lost (or approximated) in zero-dimensional studies, the remainder of this section is devoted to displaying some subtle, but often important, space-energy coupling phenomena that occur in the excore regions of LWR systems (in this case a small BWR system).

As indicated above, the 47-group data from the actual calculations are collapsed to three broad groups for presentation purposes and, in some cases, 'effective' 1-group parameters are also given. The spatially dependent data focus on the radial distributions in the reactor's pressure vessel (PV) and the concrete biological shield (bioshield) at a height of 360 cm above the bottom of the reactor vessel, and on the axial profiles at the core shroud, PV linear, and bioshield surface. Measured activity data for several isotopes are available from the JPDR experimental program at these locations. Flux, cross section, and reaction rate profiles are highlighted in the following discussion.

In particular, Fig. 4 shows several typical radial and axial broad-group flux profiles obtained from the JPDR computational model. Group 1 represents fast neutrons above 0.1 MeV, Group 3 is the thermal group with energies below 0.4 eV, and Group 2 covers all energies between these limits. The radial profiles in Fig. 4 are for a height of 360 cm, which corresponds to the location where the measured horizontal distribution of the ^{60}Co activity within the pressure vessel is available. The axial profiles are located at the core shroud and at the inner surface of the vessel and bioshield regions. Although the profiles behave qualitatively as expected, they also illustrate, quite clearly, the rapid changes in neutron spectra that occur at various locations throughout the excore regions.

The radial plot clearly shows the attenuation of thermal neutrons in the thick vessel structure and the thermalization of the hard spectrum on the surface of the bioshield with only about 10-20 cm penetration into the shield region. Similar effects can be seen in the axial profiles as one moves farther from the core region. Although spectral changes in the axial direction at any given radial location are relatively small, the changes observed when moving radially outward from the shroud, to the vessel surface, to the surface of the bioshield are indeed significant.

The impact of these spectral shifts can be illustrated by computing the effective activation cross sections versus position, taking into account the explicit change in the multigroup weight function at each spatial point. A few typical examples are given in Figs. 5, 6, and 7 which show the effective 1-group activation cross section versus position corresponding to the flux profiles given in Fig. 4. In particular, Fig. 5 shows the space dependent 1-group ^{59}Co n,γ cross section and Fig. 6 displays the same activation cross section for ^{54}Fe. These reactions are particularly important since they lead to the generation of ^{60}Co and ^{55}Fe, respectively, through

neutron activation over the life of the plant. These isotopes are two of the more important radioactive species in terms of total activity for several years after shutdown.

Finally, Fig. 7 shows the space dependence of the ^{54}Fe n,p reaction which produces ^{54}Mn with a half-life of 312.2 days. This cross section was chosen for display because it is a high-energy threshold reaction that is insensitive to thermal spectrum changes. It is, however, sensitive to the fast flux distribution and to the relative contribution of the fast component to the total energy integrated flux at a particular location. This latter dependence is due to the choice of presentation mode here - where the 'effective' cross section is always averaged over all energy. This averaging process is performed only as a mechanism for summarizing a lot of information into a single quantity. The full multigroup reaction data are used in all activation calculations.

The key observation from Figs. 5-7 is the large variation in the effective cross section versus position for all the isotopes and locations chosen here. Note, for example, that the 1-group average cross section for ^{59}Co varies by about a factor of 4-5 in the two radial regions shown in Fig. 5 (pressure vessel and bioshield regions) and by a factor of two or more in specific axial regions. This type of variability is typical (as shown in Figs. 6 and 7), and it simply indicates that large spectral shifts do occur. This phenomenon is certainly significant and it must be treated with care if reliable activation calculations are desired. Since the ACTIV code models this space-energy coupling in full detail, all the uncertainty related to the use of zone and energy averaged cross sections in the usual zero-dimensional activation analyses is eliminated completely.

The variation in the effective 1-group cross sections is an indication of changing neutron spectra. The quantity actually used in the activation calculations is the micro reaction rate with units of reactions/sec per atom. This parameter is just the reaction cross section times the flux integrated over energy. The spatial variation of the reaction rate per atom for the same reactions and locations as above is illustrated in Figs. 8, 10, and 12, respectively, for the ^{59}Co n,γ, ^{54}Fe n,γ, and ^{54}Fe n,p production reactions. These data include both spectral variations and the spatial attenuation of the total neutron flux. The spectral component of the reaction rate information can be isolated by plotting the fractional contribution of each energy group to the total reaction rate. This has been done for the ^{59}Co n,γ and ^{54}Fe n,γ reaction rates in Figs. 9 and 11, respectively. A similar plot for ^{54}Fe n,p was not very informative since it only confirmed that the fractional component for the fast group is identically unity at all spatial points (the ^{54}Fe n,p reaction has a high energy threshold above 0.1 MeV).

There is a significant amount of information contained in Figs. 4-12. These details are not generally available and they are not really essential to the user. However, with this information, a lot of insight into the physics of the activation calculation can be obtained, especially relative to the importance of the space and energy coupling in typical LWR systems (compare Figs. 9 and 11, for example). However, what is critically important is that these effects be properly treated within the activation computation. If care is taken by the user, these phenomena can be approximately incorporated manually within zero dimensional codes (such as ORIGEN). The ACTIV code, on the other hand, automatically does this without specific knowledge or interaction from the user. All important effects are treated from basic physics principles within the limitations of the multigroup activation analysis library (47 energy groups in this case).

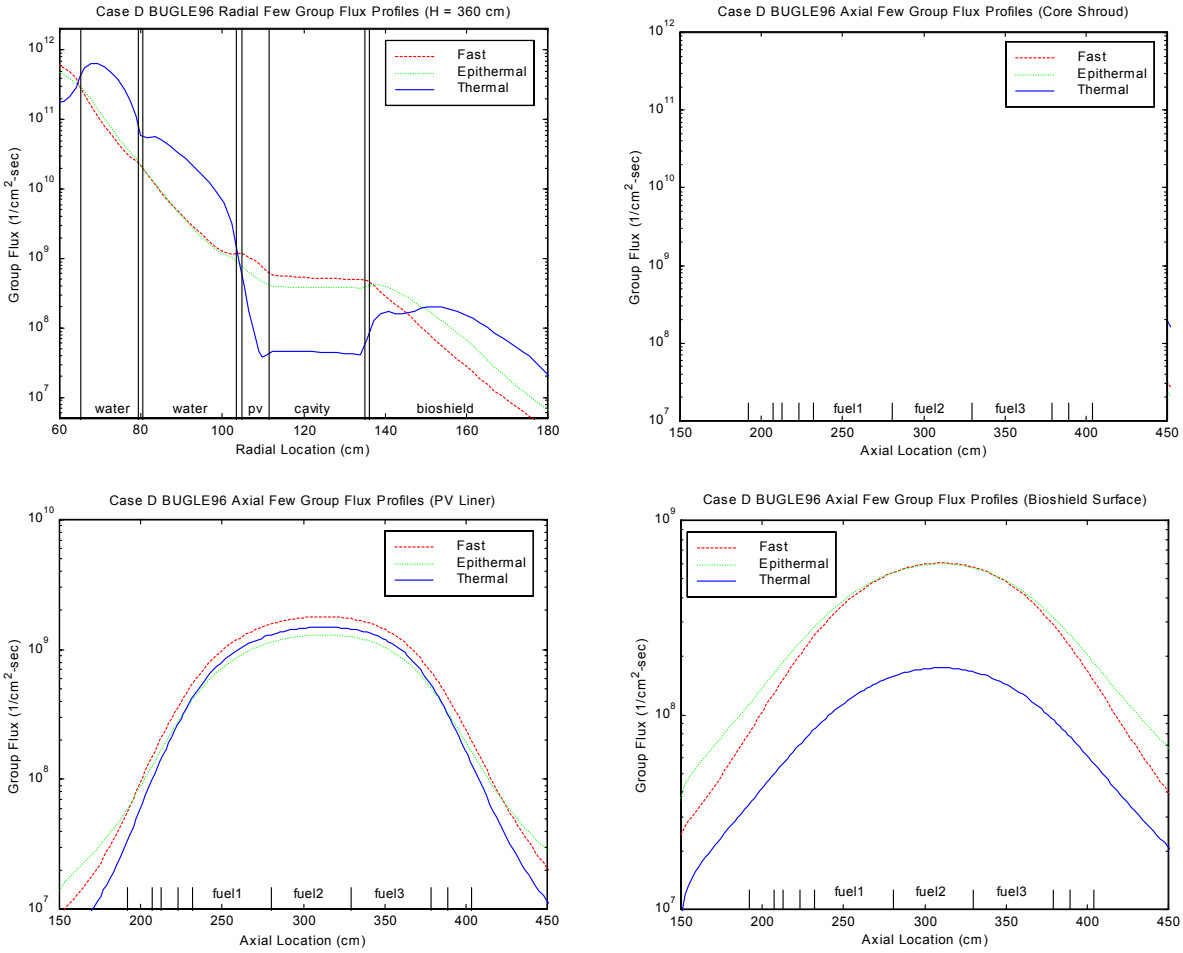

Fig. 4 Selected broad-group radial and axial flux profiles from the JPDR Case D model.

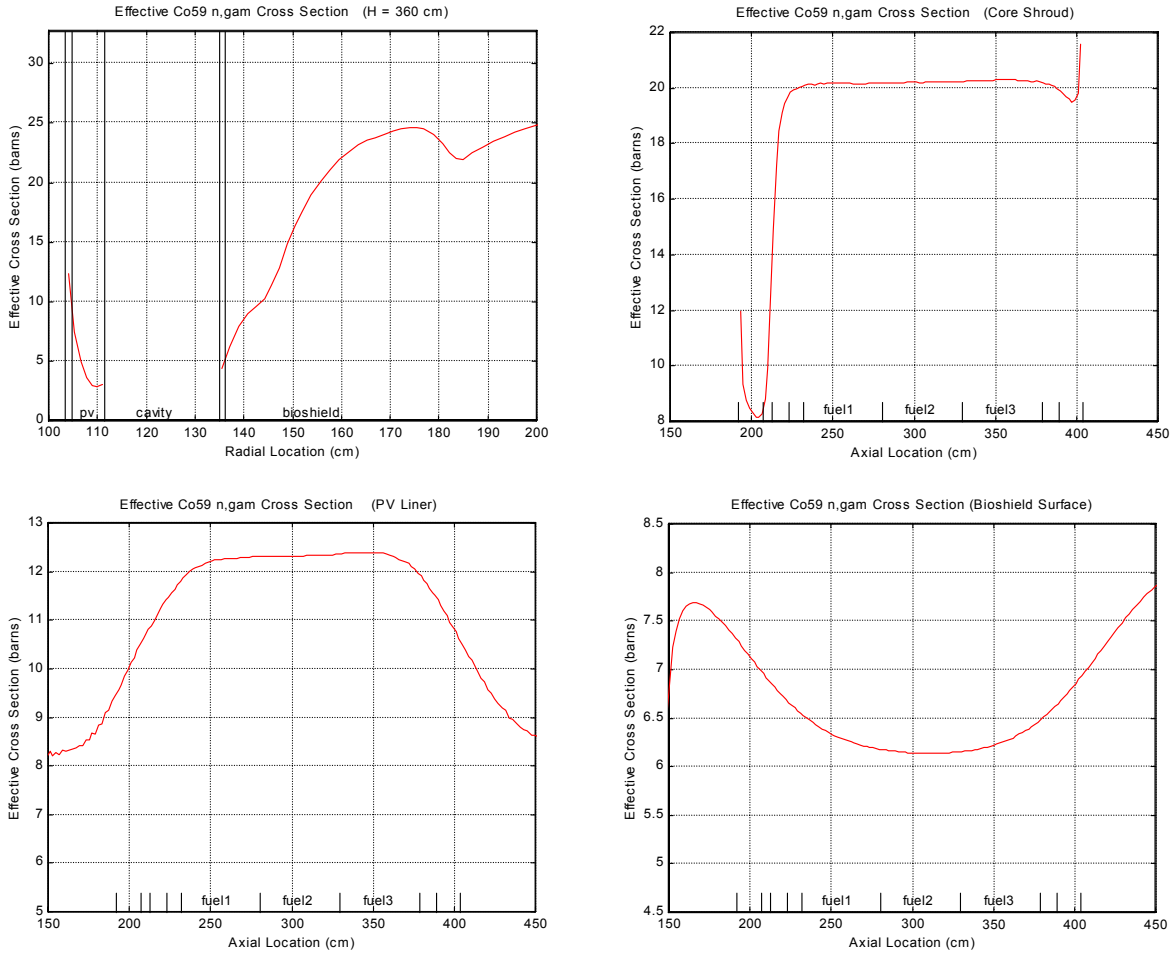

Fig. 5 Selected ^{59}Co n,γ effective cross section profiles from the JPDR Case D model.

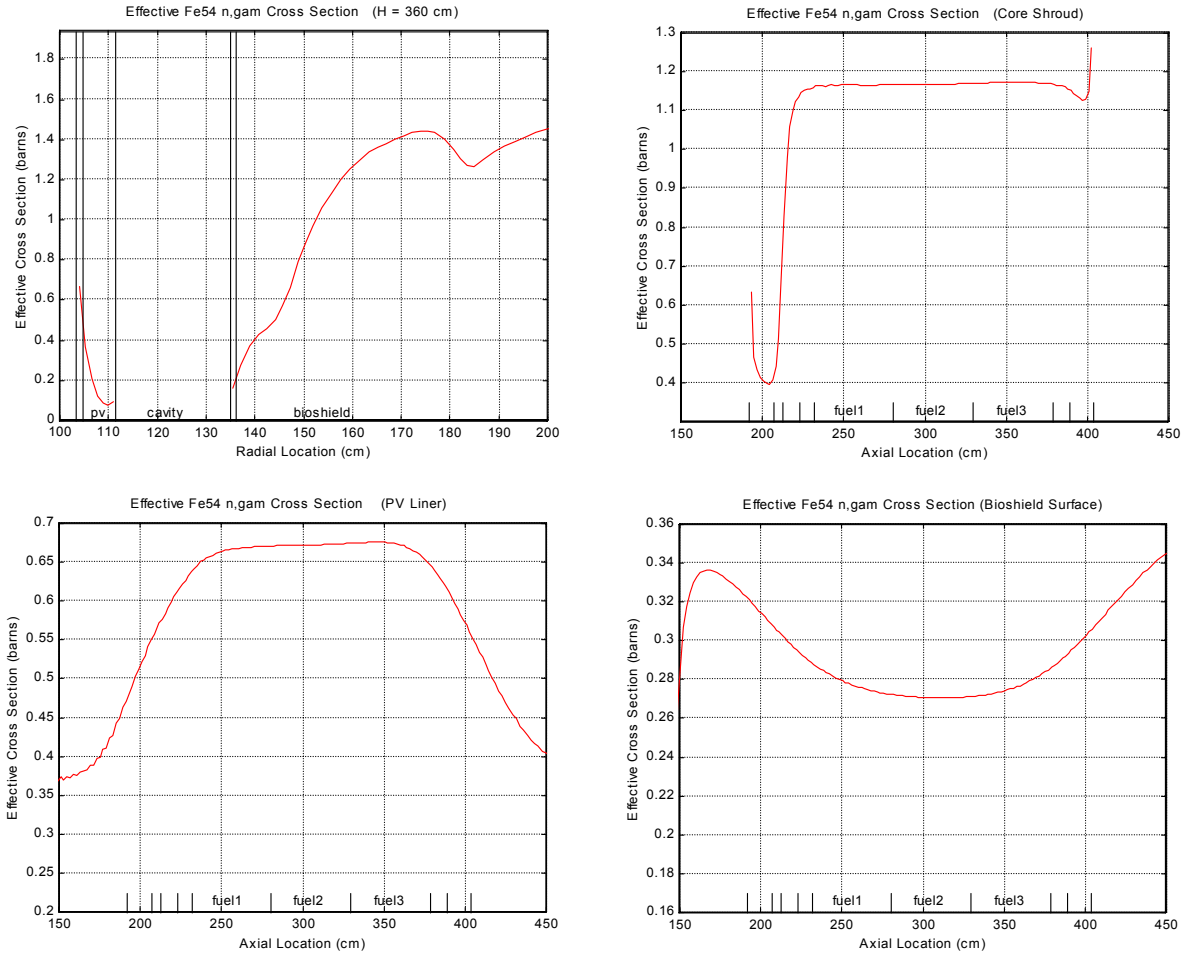

Fig. 6 Selected ^{54}Fe n,γ effective cross section profiles from the JPDR Case D model.

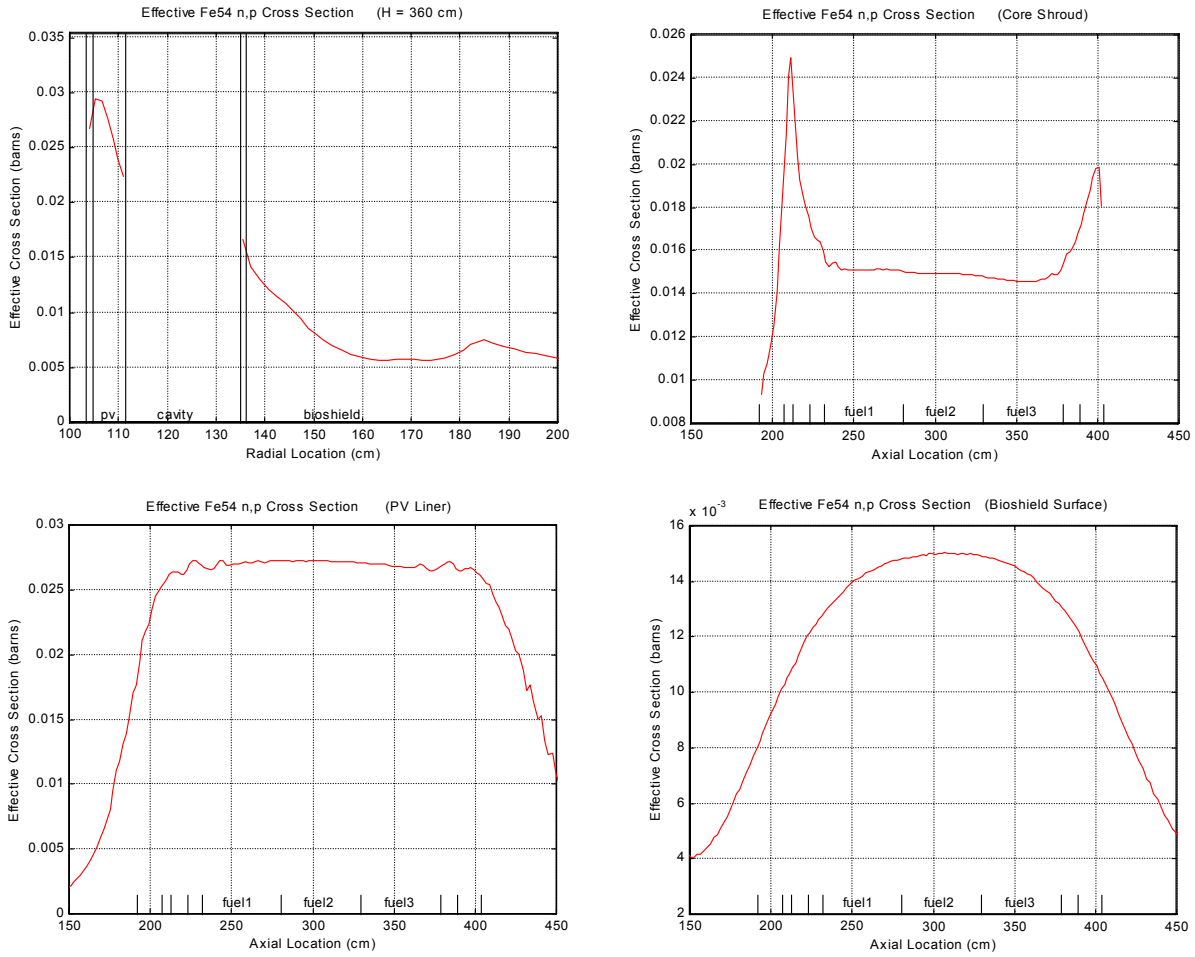

Fig. 7 Selected ^{54}Fe n,p effective cross section profiles from the JPDR Case D model.

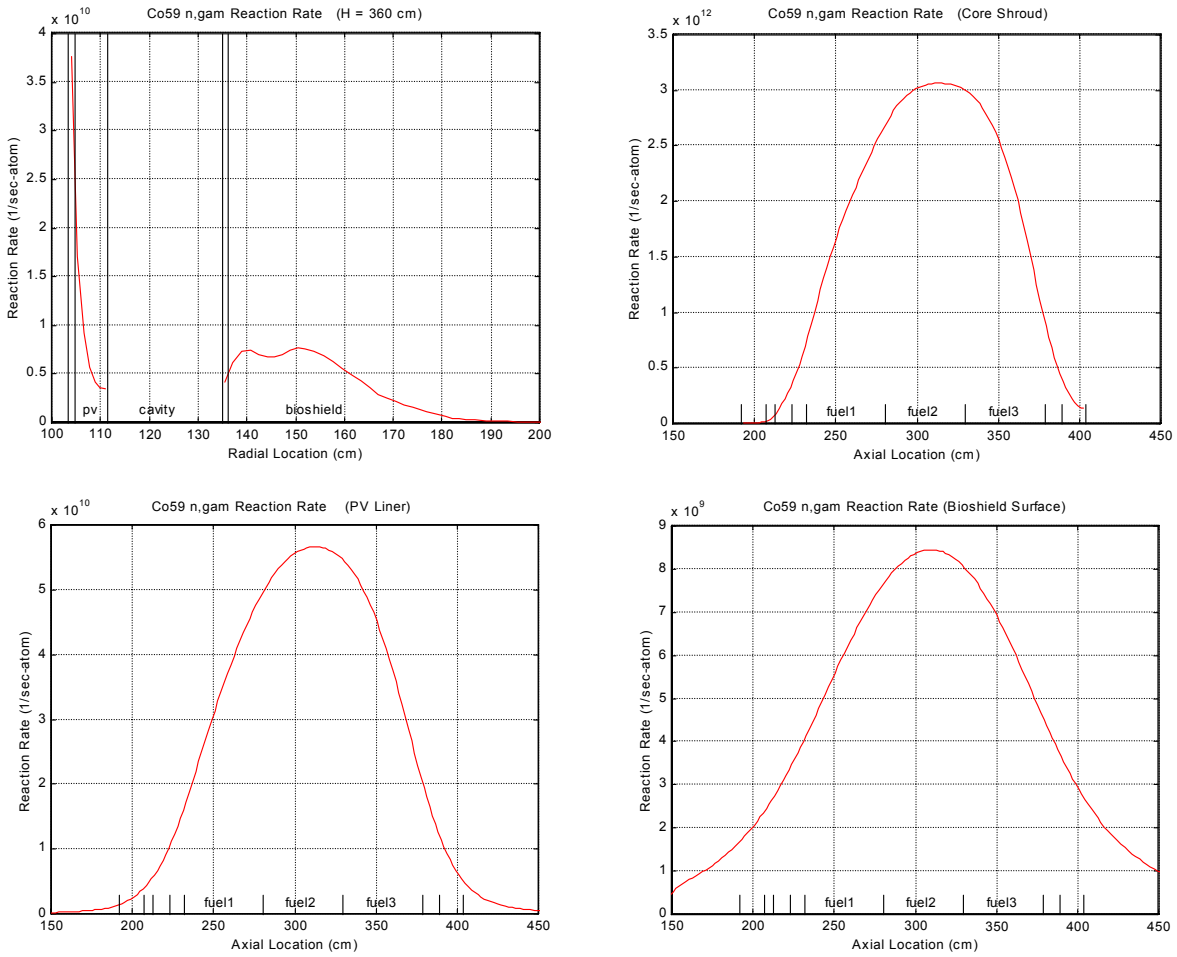

Fig. 8 Selected ^{60}Co n,γ reaction rate profiles (reactions/sec per atom) for the Case D model.

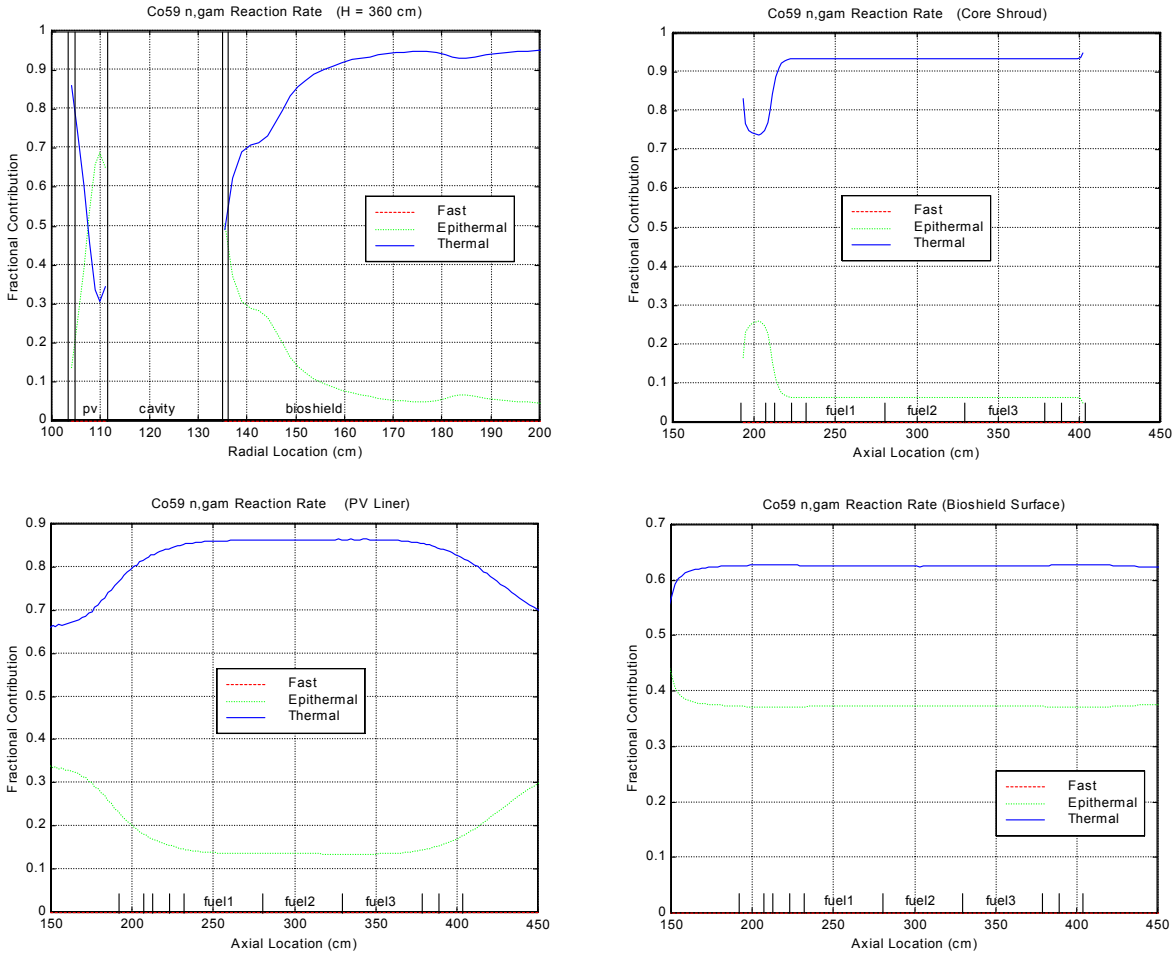

Fig. 9 Fractional contribution by broad group for the ^{60}Co n,γ reaction rate profiles.

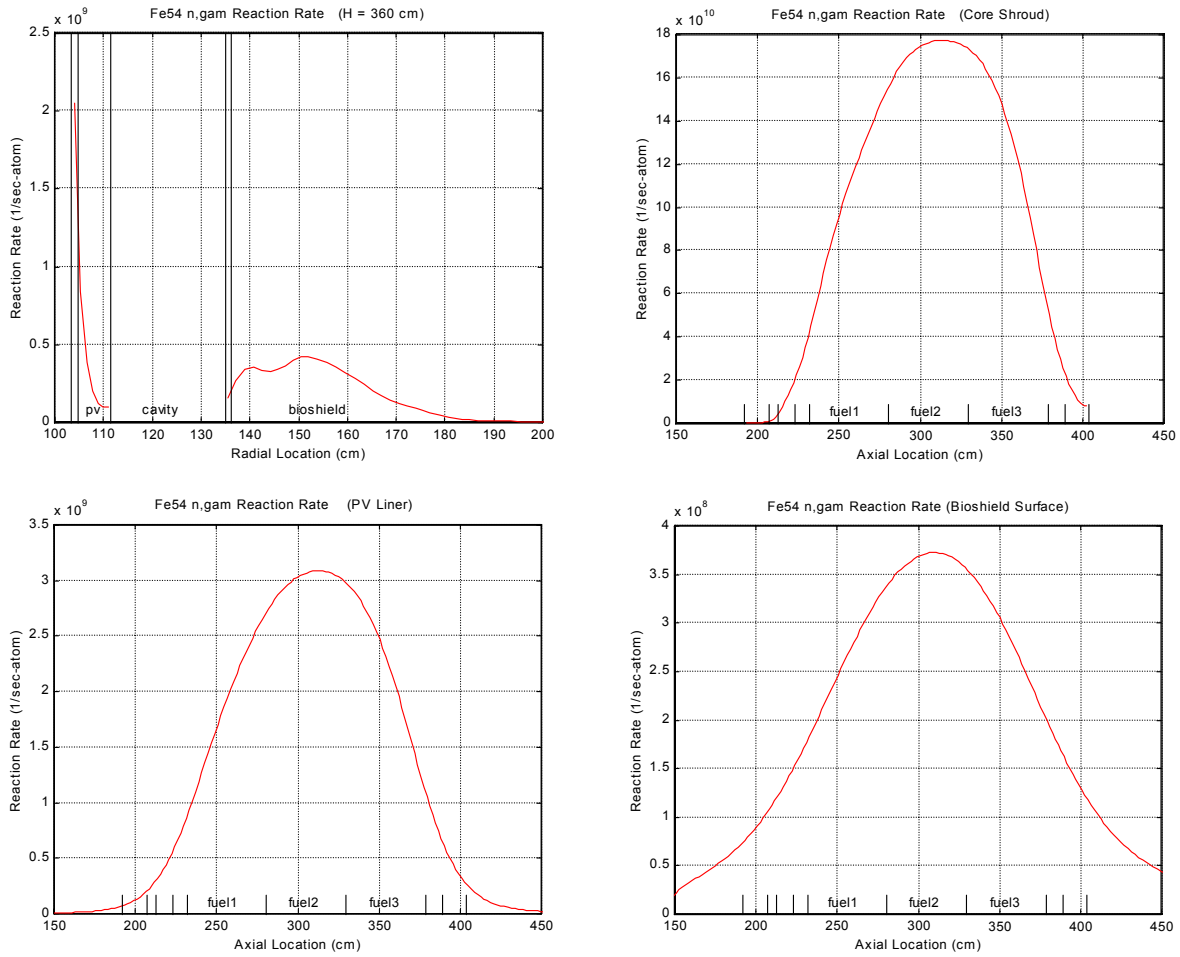

Fig. 10 Selected ^{54}Fe n,γ reaction rate profiles (reactions/sec per atom) for the Case D model.

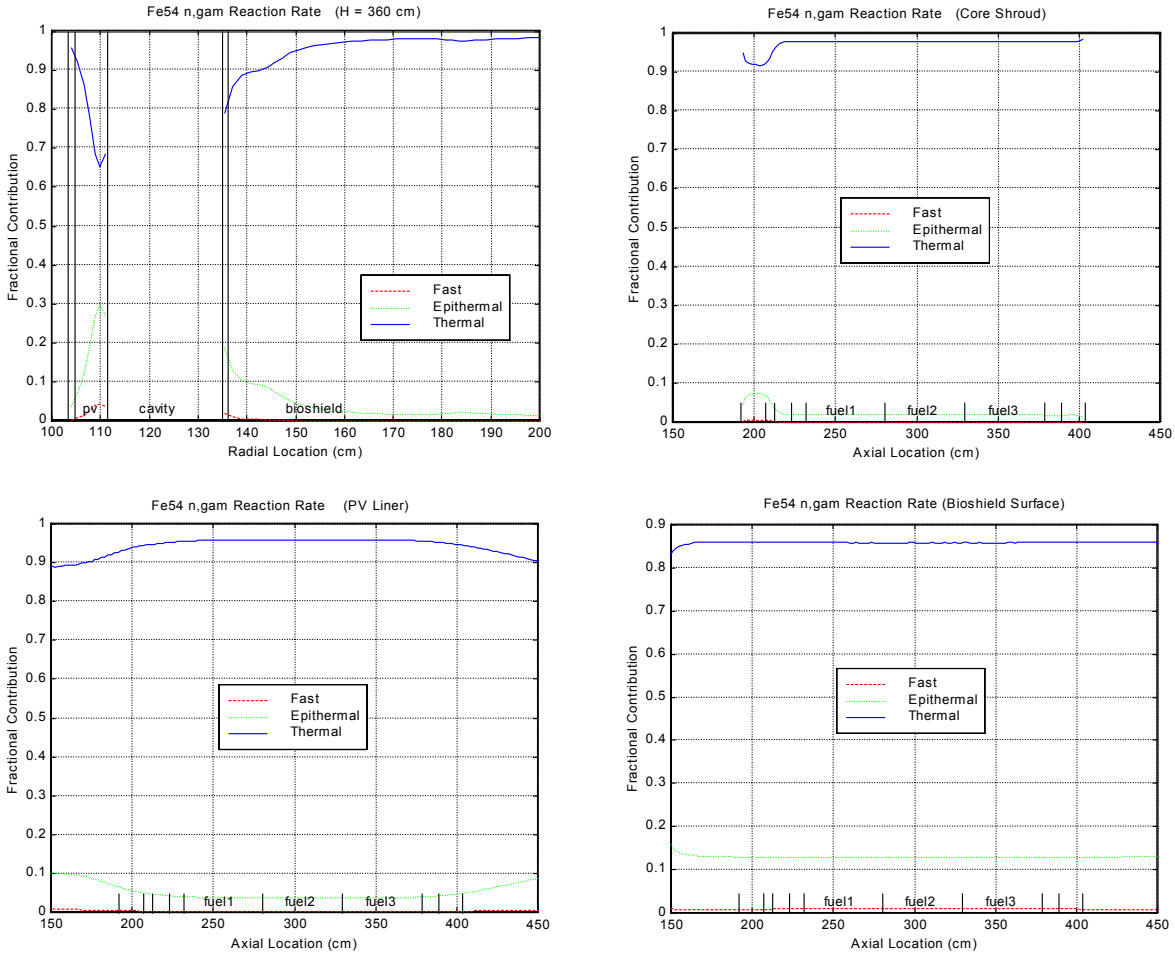

Fig. 11 Fractional contribution by broad group for the ^{54}Fe n,γ reaction rate profiles.

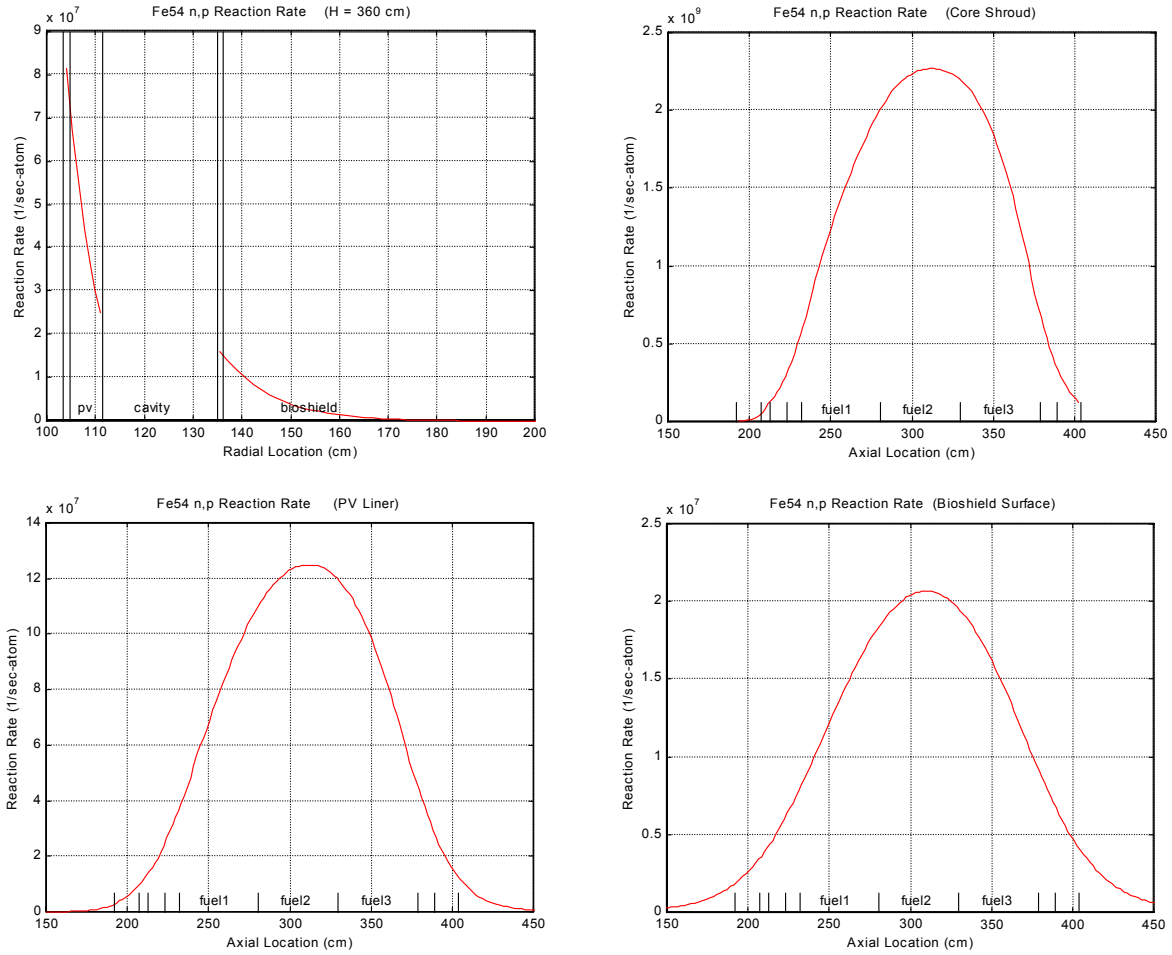

Fig. 12 Selected ^{54}Fe n,p reaction rate profiles (reactions/sec per atom) for the Case D model.

Activation Analysis Results

Using the 47-group fluxes from the DORT run and the 47-group activation cross sections in ACTXS47.LIB, ACTIV was run using the chain and decay data given in Table 2 and the initial parent densities given in Table 3. The current calculations focus on the activities associated with ^{54}Mn, ^{55}Fe, ^{60}Co, ^{63}Ni, ^{152}Eu, and ^{154}Eu because these were measured as part of the experimental program in the JPDR. The activity of ^{134}Cs was also measured at selected locations within the bioshield, however, its parent isotope, ^{133}Cs, is not available in the current VITAMIN-B6 library. Therefore, the activity associated with ^{134}Cs could not be included in this study.

Table 2. Nuclide chain and decay data used in ACTIV.

Parent Isotope	Abundance (a/o)	Daughter Isotope	Half-life (days)	Process
^{54}Fe	5.81	^{54}Mn	3.1215+2	n,p
^{54}Fe	5.81	^{55}Fe	9.9711+2	n,γ
^{59}Co	100	^{60}Co	1.9248+3	n,γ
^{62}Ni	3.59	^{63}Ni	3.6562+4	n,γ
^{151}Eu	47.9	^{152}Eu	4.8680+3	n,γ
^{153}Eu	52.1	^{154}Eu	3.1377+3	n,γ

Table 3. Initial parent densities for various activation materials in the JPDR.

Parent Isotope	SUS27 Core Shroud		ASTM-A167 Vessel Clad		ASTM-A302B Pressure Vessel		Bioshield Concrete	
	7.90 g/cc		7.90 g/cc		7.85 g/cc		2.30 g/cc	
	w/o or ppm	atom density	w/o or ppm	atom density	w/o or ppm	atom density	w/o or ppm	atom density
^{54}Fe	70.7*	3.495-3	71.4*	3.530-3	97.4*	4.785-3	1.9*	2.735-5
^{59}Co	1300	1.048-4	1200	9.677-5	200	1.603-5	6.2	1.456-7
^{62}Ni	9.2*	2.675-4	9.8*	2.849-4	0.55*	1.589-5	.0013*	1.100-8
^{151}Eu							0.59	2.575-9
^{153}Eu							0.59	2.801-9

* These entries represent weight percent and the remaining (unstarred) values in this list have units of parts per million (ppm), where both the w/o and ppm values refer to the naturally occurring material (not the specific isotope). Also, the atom densities are in atoms/b-cm.

The abundances and decay data in Table 2 came directly from the ORIGEN data libraries from SCALE4.3.[11] The initial parent concentrations in Table 3 were taken from Table 2 of Ref. 2. These data were then converted to atom densities (atoms/b-cm) for use in ACTIV. For example, if the base information is given in weight percent, one has

$$N_{ij} = \rho_j \times \frac{w_{kj}}{100} \times \left(\frac{a_i}{100} \times \frac{MW_i}{MW_k} \right) \times \frac{.60225}{MW_i}$$

where

N_{ij} = atom density (atoms/b-cm) of isotope i in material j
ρ_j = mass density (g/cm^3) of material j
a_i = atom percent abundance of isotope i in element k
w_{kj} = weight percent of natural element k in material j
MW_i = molecular weight of isotope i (g)
MW_k = molecular weight of element k (g)

If parts per million (ppm) is given instead of weight percent (w/o), one simply replaces (w_{kj}/100) with ($ppm_{kj}/10^6$) in the above equation.

The power versus time history for the ACTIV calculation was taken from Fig. A.4 of Ref. 2. There were ten alternating periods of constant power operation and full shutdown, with the last shutdown period lasting 15 years. This latter time interval represents the time from when the reactor was shutdown permanently to when the activation measurements were made. The total simulation time, from initial startup of the JPDR to the measurement time, was 10011.8 days. Thus, all subsequent activation results are reported for this point in time (relative to startup at time zero).

With all this background to establish some specificity to the actual computations that were performed, we can now finally show some of the calculated activities, with a direct comparison to the data measured in the JPDR decommissioning program. The key results and comparisons discussed here are broken into four parts which highlight the following:

I. The radial activity profiles in the vessel and bioshield,

II. The axial activity distribution in the core shroud,

III. The axial activity profiles in the PV liner, and

IV. The axial distribution of activities along the surface of the bioshield.

I. The Radial Profiles

The radial profiles focus exclusively on the ^{60}Co activity, first in the pressure vessel and then in the bioshield. These data are plotted in Figs. 13 and 14. Each figure comparing the calculated and experimental radial activities has two components. The first part shows a plot of the absolute activities, with the circles representing the measured values and the solid line giving the computed values. The second figure in each set displays the behavior of the ratio of the calculated-to-experimental value (C/E value) with the asterisks showing the actual C/E value at each measurement location and the solid line representing a low-order best fit to these individual points. For the pressure vessel (see Fig. 13), a quadratic fit was used and, in the bioshield (see Figs. 14), a simple linear fit was used for the C/E profile. The fits were used to simply show the general trend in the C/E data.

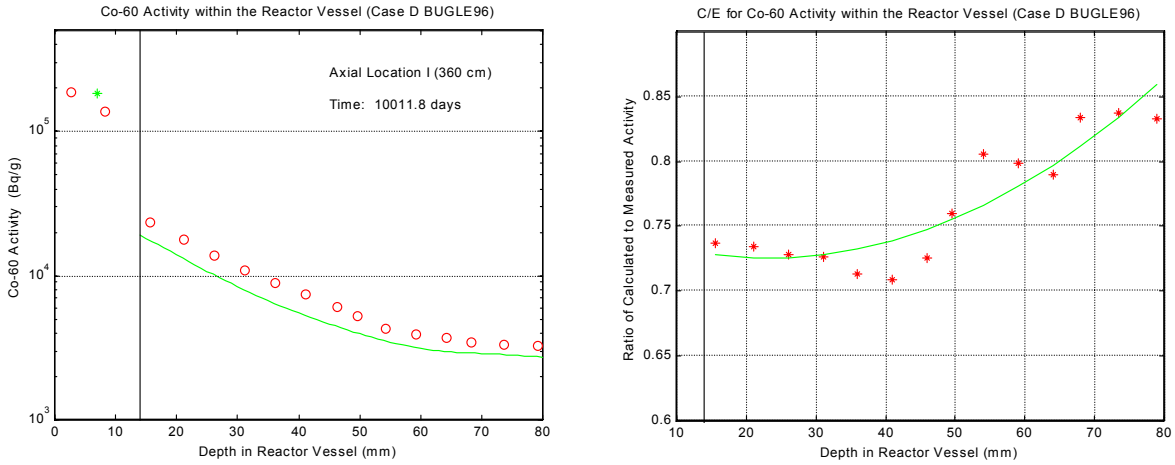

Fig. 13 Radial activity and C/E profiles for ^{60}Co within the reactor vessel.

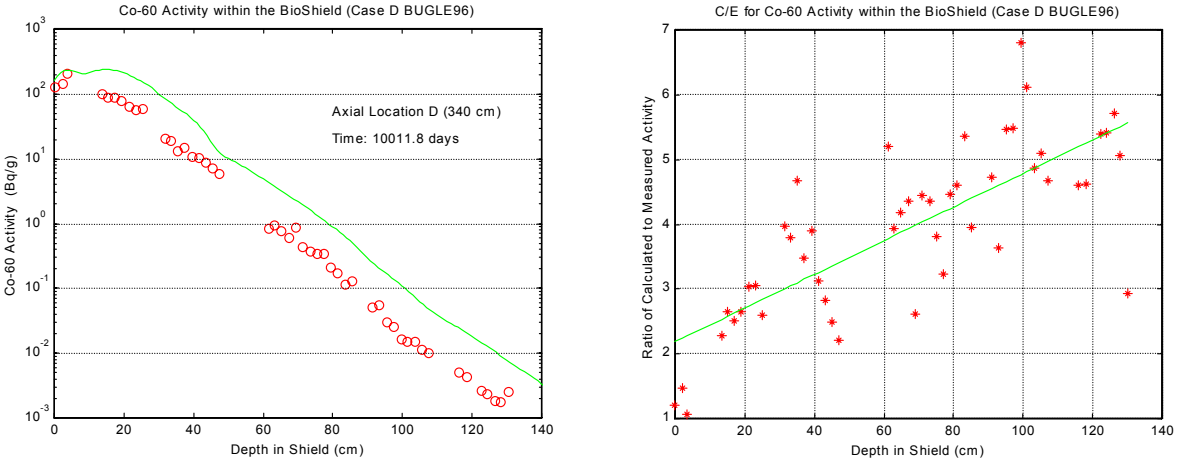

Fig. 14 Radial activity and C/E profiles for ^{60}Co within the bioshield.

II. The Axial Profiles at the Core Shroud

The axial activity data for the core shroud are summarized in Figs. 15 and 16 and in Table 4. Four radioactive isotopes are highlighted - ^{54}Mn, ^{55}Fe, ^{60}Co, and ^{63}Ni. Figure 15 again shows the experimental data as points and the calculated profiles as solid curves. Since there are only three measured values for each profile, the numerical values of the C/E ratios have been tabulated in Table 4. Also of interest is the profile of the activity ratio relative to the ^{60}Co activity. This quantity is quite useful in practice since the ^{60}Co activity can often be inferred from gamma scans of the various excore components. Figure 16 displays the computed axial profiles of several activity ratios at the core shroud along with the experimental values obtained from the JPDR measurement program.

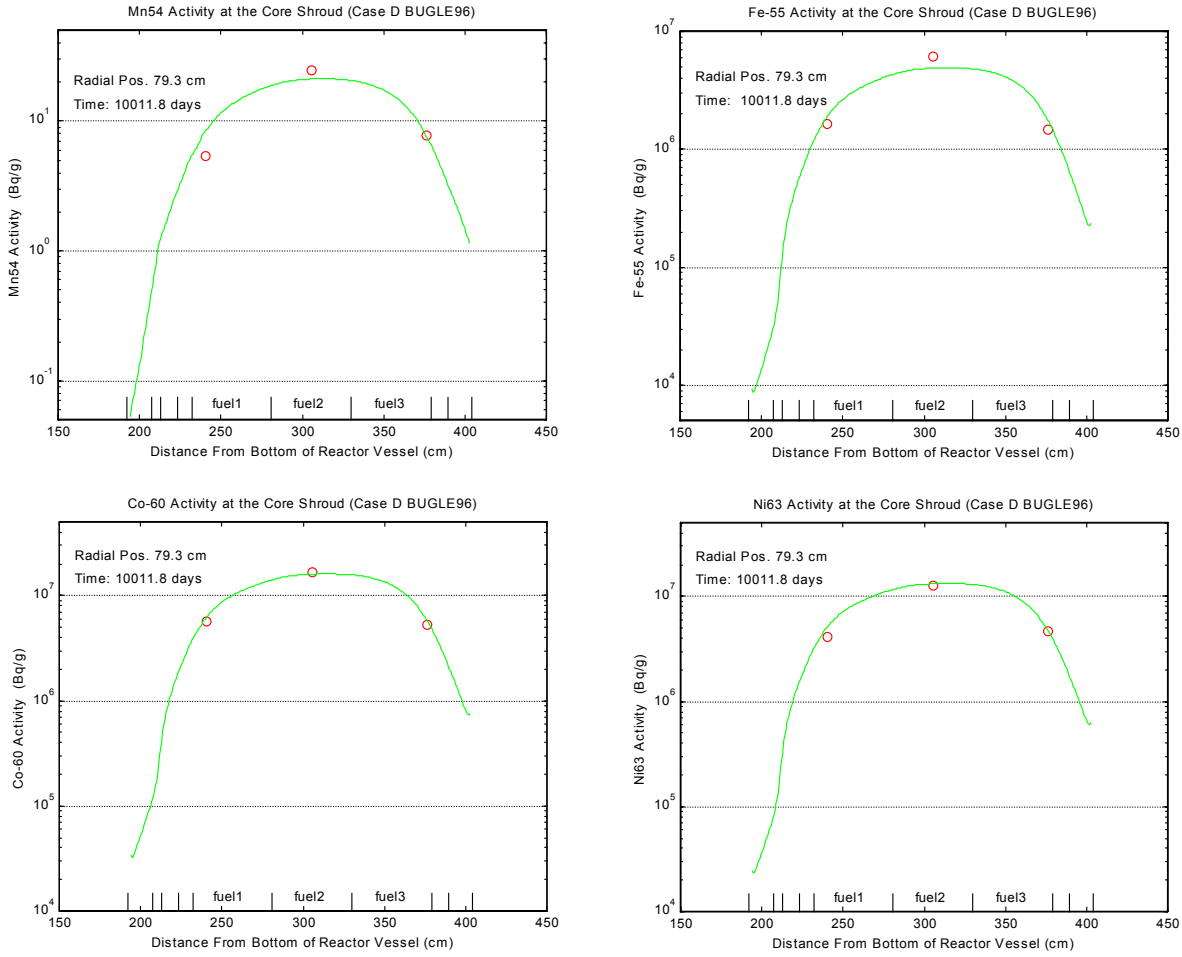

Fig. 15 Several axial activity profiles at the core shroud.

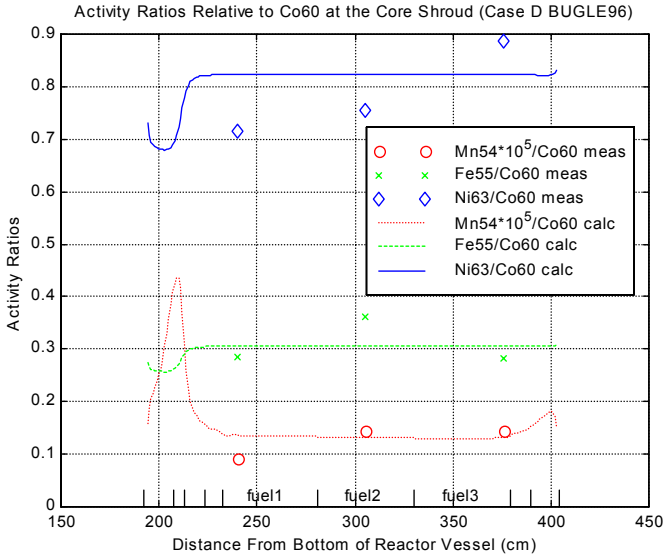

Fig. 16 Axial profiles of the relative activities at the core shroud.

III. The Axial Profiles at the Reactor Vessel

The axial activity data for the pressure vessel are summarized in Figs. 17 and 18 and in Table 5. These presentation aids organize the important computational and experimental data in exactly the same format as for the core shroud - only this time the calculated profiles and C/E data are for the radial mesh point associated with the pressure vessel liner. Also, these data include five measured data points for each activity profile.

IV. The Axial Profiles at the Surface of the Bioshield

The calculated axial activity profiles for ^{60}Co, ^{152}Eu, and ^{154}Eu at the surface of the concrete bioshield are displayed in Fig. 19. Explicit experimental data in the axial direction are not available for comparison here. However, the first few points for the radially dependent experimental data at a height of 340 cm above the bottom of the reactor vessel were used to linearly interpolate a single value at a radius of 137.2 cm. This single 'measured' data point is shown as a circle in the three curves in Fig. 19. This point was included just to show that the computed profiles are reasonable relative to measured data (at least from an overall normalization perspective).

Table 4. C/E values at several axial points along the core shroud.

	Point 1	**Point 2**	**Point 3**
^{54}Mn	1.51	0.85	0.99
^{55}Fe	1.10	0.79	1.20
^{60}Co	1.03	0.93	1.11
^{60}Ni	1.18	1.01	1.03
z location (cm)	240	305	376

Table 5. C/E values at several axial points along the reactor vessel.

	Point 1	**Point 2**	**Point 3**	**Point 4**	**Point 5**
^{54}Mn	1.91	1.09	1.29	1.18	1.31
^{55}Fe	1.16	0.74	0.88	0.86	0.90
^{60}Co	1.13	0.70	0.83	0.81	0.84
^{60}Ni	1.07	0.69	0.82	0.80	0.84
z location (cm)	206	256	306	328	368

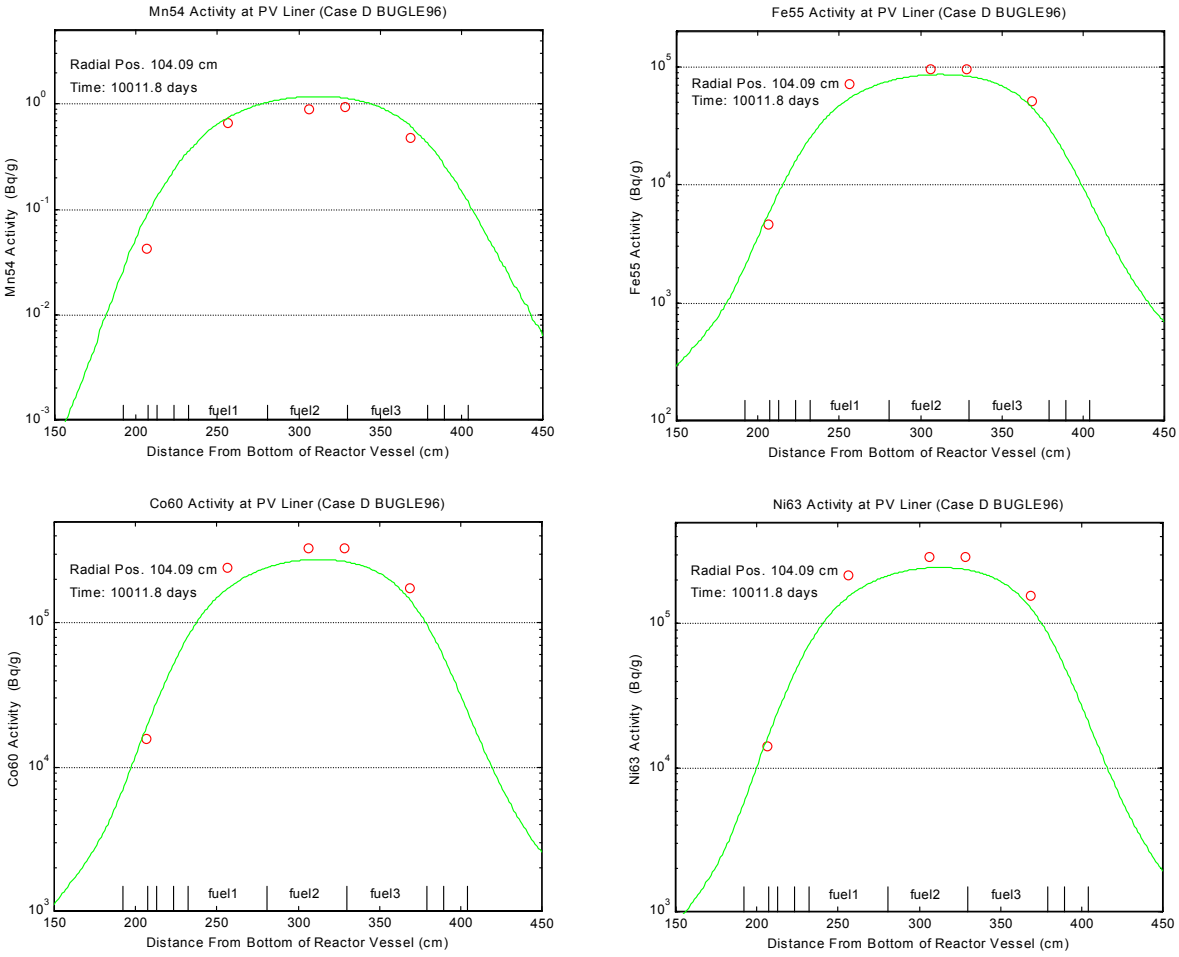

Fig. 17 Several axial activity profiles at the PV liner.

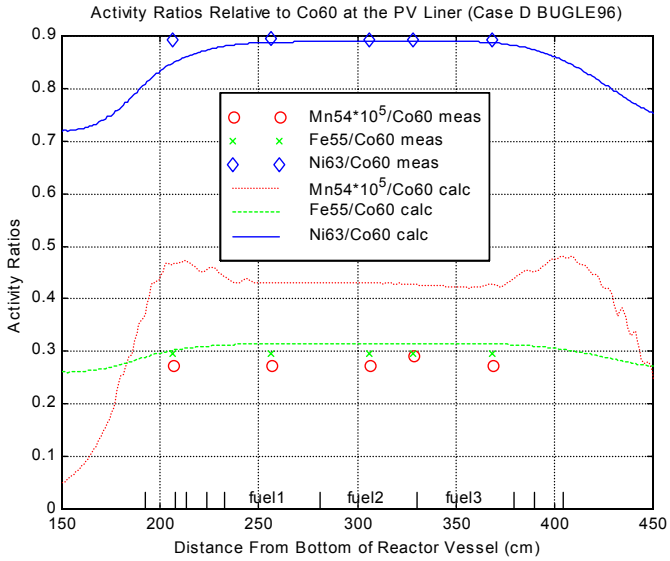

Fig. 18 Axial profiles of the relative activities at the PV liner.

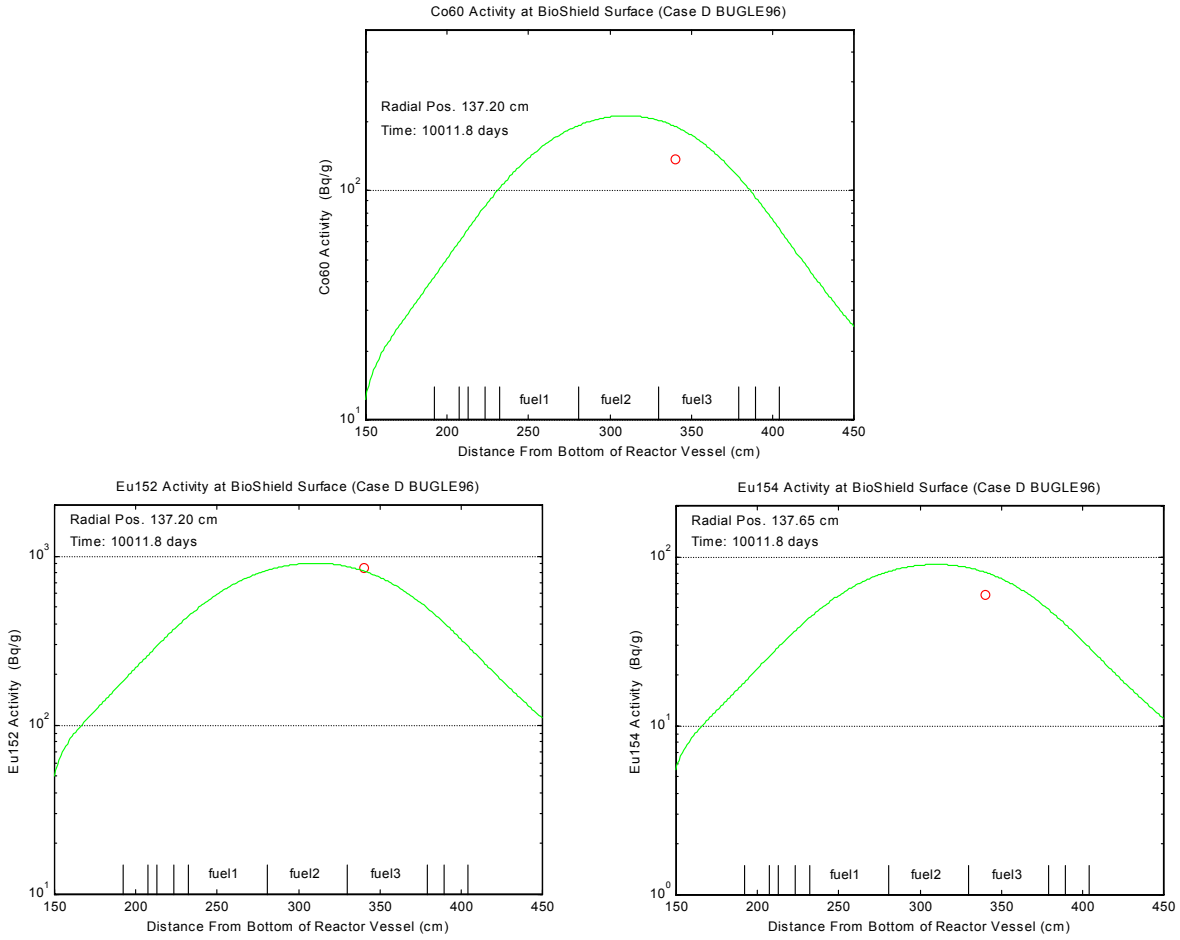

Fig. 19 Several axial activity profiles at the surface of the concrete bioshield.

Discussion of the Results

Shroud and Vessel Regions

Concerning the plots and tabular data, one can easily argue that very good results were obtained for most radial and axial points through the pressure vessel region of the JPDR model. There is certainly a lot of information contained in Figs. 13 and 15-18 and in Tables 4 and 5, and most of it suggests that the DORT-ACTIV calculational sequence does a good job in predicting the activity in the shroud and reactor vessel relative to measured data from the JPDR experimental program. For example, the C/E values in Fig. 13 show that the radial distribution of the ^{60}Co activity is under-predicted by 15% to 30% (C/E range is from 0.85 to 0.70). Also most of the axial profile C/E values in Tables 4 and 5 show agreement with experiment to within ±30% (C/E values range from 0.70 to 1.30), with many values reasonably close to unity.

The only real exception to the above discussion is associated with the ^{54}Mn activity at the lowest measured point in both the shroud and PV liner. In both cases, the DORT-ACTIV computations significantly over-predict the ^{54}Mn activity relative to measured values (by 50% at the shroud and by 90% in the vessel). This apparent discrepancy is of concern, and no single good explanation for the large error is available. However, it should be emphasized that the

absolute ^{54}Mn activity is very low relative to the other measured activities (by 5-6 orders of magnitude), that the parent reaction, an ^{55}Fe n,p interaction, has a high energy threshold, and that only the lowest measurement point (in the vicinity of the axial plane associated with the lower grid and support plate) has this problem. Clearly the modeling and homogenization approximations needed in this area could be the culprit. Also of note is that no uncertainty information is available for any of the measured data or the material concentrations given in Ref. 2. Thus, with all these considerations, it is important not to place too much significance in the poor agreement for these two data points - but they should not be simply ignored either.

One final note relative to the results obtained within the shroud and vessel concerns the activity ratios given in Figs. 16 and 18. First note that the variation in the experimental ratios along the axial region associated with the core (see especially Fig. 16) is probably a rough measure of the uncertainty of the data. Also, in general, very good agreement with the 'measured' ratios was observed. This is important since this type of information is used frequently in practical application and the ability to accurately compute various activity ratios relative to the ^{60}Co activity is critical.

One exception to this good agreement is apparent in Fig. 18 for the ^{54}Mn/^{60}Co activity ratio in the PV liner. The large over-prediction (roughly 0.43E-5 versus 0.28E-5, respectively, for the calculated and measured activity ratios in the axial plane associated with the core) is due to the high computed activities for ^{54}Mn and the general under-prediction of the ^{60}Co activity. Again, the cause of this discrepancy is not clear. However, the high energy threshold for the ^{55}Fe reaction and the sensitivity of the high energy component of the flux to various modeling assumptions may be contributing factors. The very small absolute value for this ratio may also prevent an accurate numerical evaluation.

Thus, except for a few anomalies, the general accuracy of the calculations, up to and including the vessel, is on the order of ±30%. This is considered a fairly impressive finding, especially considering the complexity of the calculations required to produce these comparisons. In addition, although not explicitly stated, it is expected that the experimental data and the initial isotopic concentrations in the structural materials have combined uncertainties approaching, or possibly exceeding, the range of C/E values determined within the vessel of the JPDR configuration.

Bioshield Regions

The good agreement that was observed up through the vessel was not achieved in the bioshield region. Good accuracy was obtained at the bioshield surface, but the DORT-ACTIV calculations significantly over predict the measured activity at all points in the bioshield, and the error tends to grow with distance into the shield, approaching a factor of about 5 at approximately 100 cm into the shield. These statements are supported by Figs. 14 and 19. This general behavior is consistent for all the isotopes.

The poor agreement of the computed bioshield activities relative to measured values is attributed to the relatively cursory modeling information available for this portion of the JPDR. Although Ref. 3 improved upon the bioshield data from Ref. 2, there still is too much uncertainty in the precise geometry, concrete water content, measurement locations, etc., to allow adequate comparisons and conclusions to be drawn. A number of sensitivity computations were

performed to try to isolate the key parameters, but even these were inconclusive because of inadequate modeling and operational information.

The above general remarks concerning the utility of the JPDR bioshield data are consistent with other researchers (see Refs. 8 and 9 , for example). The conclusion, therefore, is simply that there is too much uncertainty in the JPDR bioshield geometry and operational data for it to be useful in the current DORT-ACTIV verification exercise. Further information from the JPDR experimental program or from some other source is needed for additional testing in the bioshield region. This is definitely an area that needs further work in the future.

Overall Summary

This report summarizes the data, methods, models, and codes used to generate the latest UMass-Lowell JPDR benchmark results. It represents a verification benchmark for the DORT-ACTIV sequence using the VITAMIN-B6 and BUGLE96 data libraries. A comparison of the computed and measured activities for several isotopes included as part of the JPDR experimental program shows good agreement for most data points up to and including the reactor vessel, with a variability of about ±30%.

A few anomalous points with high computed values were observed for the ^{54}Mn activity. The high energy threshold reaction in ^{55}Fe that produces ^{54}Mn makes this activity very sensitive to data uncertainties and modeling approximations.

The JPDR bioshield data were not included in the present verification because of the large modeling and geometry uncertainties that exist. Additional studies are needed for conformation that the DORT-ACTIV sequence can adequately predict individual isotope activities well into the bioshield region.

Overall, the current benchmark exercise successfully validates the general computation procedure and data libraries used in the present analyses. There are several areas that could use further study and additional validation (bioshield region, ^{54}Mn activity, other isotope activities, additional data comparisons in axial regions farther from the core, etc.), but the base methodology has been clearly established as adequate for predicting excore activities after long term exposure to a neutron field. The DORT-ACTIV combination is easy to use and it treats the basic physics of neutron activation with full space energy coupling. It represents one of the most comprehensive tools for performing analyses of this type. The JPDR benchmark computations performed here successfully demonstrate the utility of this approach to activation analysis.

References

1. N. Kocherov, "Benchmark on Radioactive Inventory Calculations for Fission Reactor Decommissioning," letter from IAEA to potential participants in benchmark exercise (1994).
2. T. Sukegawa, et. al., " Accuracy Verification for Calculation of Inventory in JPDR Due to Neutron Activation," International Atomic Energy Agency, INDC(JPN)-164 (1993).
3. Letter from N. Kocherov (IAEA) to J. R. White (UMass-Lowell) dated March 31, 1995 containing detailed drawings from JAERI describing the central part of the JPDR bioshield.
4. J. R. White and A. P. Fyfe, "UMass-Lowell Results for the JPDR Activation Analysis Benchmark," 1996 Topical Meeting on Radiation Protection and Shielding, No. Falmouth, Massachusetts (April 1996).
5. "BUGLE-93 - Production and Testing of the VITAMIN-B6 Fine-Group and the BUGLE-93 Broad-Group Neutron/Photon Cross-Section Libraries Derived from ENDF/B-VI Nuclear Data," Radiation Shielding Information Computational Center, DLC-175 (1994).
6. "VITAMIN-B6 - A Fine-Group Cross Section Library Based on ENDF/B-VI Release 3 for Radiation Transport Applications," Radiation Shielding Information Computational Center, DLC-184 (1996).
7. "BUGLE-96 - Coupled 47 Neutron, 20 Gamma-Ray Cross Section Library Derived from ENDF/B-VI for LWR Shielding and Pressure Vessel Dosimetry Applications," Radiation Shielding Information Computational Center, DLC-185 (1996).
8. B. L. Broadhead and R. L. Childs, "ORNL Contribution to the IAEA Benchmark Problem on Fission Reactor Decommissioning," 1996 Topical Meeting on Radiation Protection and Shielding, No. Falmouth, Massachusetts (April 1996).
9. S. J. Wall, M. H. Dean, and N. J. France, "Current Status of UK Calculations for IAEA Decommissioning Benchmark (JPDR)," 1996 Topical Meeting on Radiation Protection and Shielding, No. Falmouth, Massachusetts (April 1996).
10. "DOORS3.1 - One, Two, and Three Dimensional Discrete Ordinates Neutron/Photon Transport Code System," Radiation Shielding Information Computational Center, CCC-650 (1996).
11. "SCALE 4.3 - Modular Code System for Performing Standardized Computer Analyses for Licensing Evaluation for Workstation and Personal Computers," Radiation Shielding Information Computational Center,CCC-545 (1997).
12. "BOLD VENTURE IV - A Reactor Analysis Code System, Version IV," Radiation Shielding Information Center Computer Code Collection, CCC-459 (1985).